

## Stochastic reorientations and the hydrodynamics of microswimmers near deformable interfaces

Sankalp Nambiar <sup>\*</sup>*Nordita, KTH Royal Institute of Technology and Stockholm University, Stockholm 10691, Sweden*J. S. Wettlaufer<sup>†</sup>*Nordita, KTH Royal Institute of Technology and Stockholm University, Stockholm 10691, Sweden  
and Departments of Earth & Planetary Sciences, Mathematics and Physics, Yale University,  
New Haven, Connecticut 06520-8109, USA*

(Received 26 June 2023; accepted 9 January 2024; published 14 February 2024)

We study the hydrodynamic interaction between a microswimmer and a deformable interface when the swimmer can stochastically reorient itself. We consider a force- and torque-free swimmer, modeled as a slender body, that can execute random orientation tumbles or active Brownian rotations in the plane of the deformable interface. When the swimmer is in the more viscous fluid, our analysis shows that both tumbles and Brownian rotations acting on timescales comparable to that of interface deformations can lead to a pusher-type swimmer rotating away from the interface, while enhancing its attraction towards the interface. In turn, the intrinsic orientational stochasticity of the microswimmer favors a stronger migration of pushers towards the interface at short times, but migration away from the interface in the long-time limit. However, irrespective of the viscosity ratio of the two fluid medium, the tendency of a pusher to align parallel to the interface is suppressed; the results for puller-type swimmers are the opposite. Our study has potential consequences for the residence time of swimming microorganisms near deformable boundaries.

DOI: [10.1103/PhysRevFluids.9.023102](https://doi.org/10.1103/PhysRevFluids.9.023102)

### I. INTRODUCTION

Swimming microorganisms inhabiting fluid spaces proximate to boundaries, interact with them for a variety of biological imperatives, such as formation of biofilm colonies and adhesion [1], navigation [2], and foraging [3,4]. Understanding these microswimmer-boundary interactions is relevant in biomedical and industrial settings in terms of biofouling resulting from the accumulation of biota [5,6], in controlling motion of artificial microbots in vascular systems [7], and in pathogenesis [8–10], to give just a few examples. An important aspect of these systems involves the fluid mediated hydrodynamics [11], both in quiescent suspensions [12,13] and in the presence of imposed flows [4,14,15].

---

<sup>\*</sup>Present address: Department of Chemical Engineering, Indian Institute of Technology Delhi, New Delhi 110016, India; [snambiar@iitd.ac.in](mailto:snambiar@iitd.ac.in)

<sup>†</sup>[jw@fysik.su.se](mailto:jw@fysik.su.se)

Published by the American Physical Society under the terms of the [Creative Commons Attribution 4.0 International](https://creativecommons.org/licenses/by/4.0/) license. Further distribution of this work must maintain attribution to the author(s) and the published article's title, journal citation, and DOI. Funded by [Bibsam](https://www.bibsam.org/).

In several settings, the boundaries are compliant [2,10,16], which requires a simultaneous treatment of the fluid- and boundary deformation fields. As highlighted by recent theoretical and computational studies [17–21], the dynamical response of such coupled interactions has consequences for swimmer navigation and migration. In addition to the hydrodynamics, these active swimmers, whether artificial [22] or biological [11], have an intrinsic ability to independently change their direction of motion, which may influence their interaction with the boundary.

Motivated by these problems, here we study the migration characteristics of a microswimmer that can intrinsically reorient itself, while it disturbs the fluid near a deformable interface. We model an infinitesimally thin interface that deforms due to surface tension and elastic bending, and consider microswimmers that execute orientation tumbles and rotational Brownian motion as exhibited, for instance, by swimming bacteria [11,23] or artificial self-propelled particles [24]. Building on our previous analysis [21], we discuss how a combination of hydrodynamic interaction induced rotation and translation of a microswimmer near a deformable interface and its intrinsic stochastic reorientations can enable it to control its migration. Specifically, we highlight how even in-plane swimmer reorientations can influence the out-of-plane reorientation, thereby modifying the swimmer migration behavior. Therefore, our study may have consequences for understanding the residence time and accumulation of swimmers near deformable boundaries.

The paper is organized as follows. In Sec. II, we briefly describe the coupled equations governing the hydrodynamic interaction between a slender swimmer and a deformable interface and then introduce the orientation-tumbling and rotational Brownian motion adopted for the intrinsic swimmer reorientations. The resulting equation for the boundary deformation and the expression for swimmer translation and rotation are given in Appendix A. The implementation of the intrinsic swimmer reorientation are discussed in Appendix B. Next, in Sec. III, we present results for the swimmer migration and interface deformation of a tumbling swimmer when it is in the more viscous fluid. We first analyze the modification to the swimmer rotation and interface deformation in Sec. III A, then its translation in Sec. III B, and lastly how the two influence its migration in Sec. III C. In Sec. IV, we discuss the regime of validity of our analysis and the microswimmer migration character over a range of fluid viscosities. Finally, we compare the microswimmer rotational response due to orientational tumbling with rotational Brownian motion before concluding with Sec. V.

## II. PROBLEM FORMULATION

The coupled hydrodynamic system considered here involves a swimmer that does not self-propel, but generates a disturbance field in the surrounding fluid medium, which in turn deforms the interface in proximity to it. The flow field generated due to the presence of the boundary can nevertheless result in a nontrivial swimmer mobility. We treat the interface as an infinitesimally thin boundary, with a prescribed surface tension and elastic bending modulus that control its deformability. The microswimmer is treated using slender-body theory, which is a reduced order model for, say, a flagellated swimming microorganism or an artificial self-propelled particle, which preserves information of its finite length and its orientable geometry [21,25,26]. The slender swimmer model approximates the origin of the activity in the system; namely, the motions on the boundary of the swimmer, to a line distribution of forces along the axial coordinate of the swimmer, as shown in Fig. 1 (see left window).

The equations for the coupled hydrodynamics have been derived recently [21], which we briefly summarize here. The fluid regions 1 and 2 are governed by the continuity equation and the Stokes equations,

$$\nabla_r \cdot \mathbf{v}_1 = 0, \quad -\nabla_r P_1 + \nabla_r^2 \mathbf{v}_1 = \frac{D\mathbf{p}}{\ln \kappa} \int_{-\frac{1}{2}}^{\frac{1}{2}} \text{sgn}(s)\delta(\mathbf{r})ds \quad \text{and} \quad (1a)$$

$$\nabla_r \cdot \mathbf{v}_2 = 0, \quad -\nabla_r P_2 + \lambda \nabla_r^2 \mathbf{v}_2 = 0, \quad (1b)$$

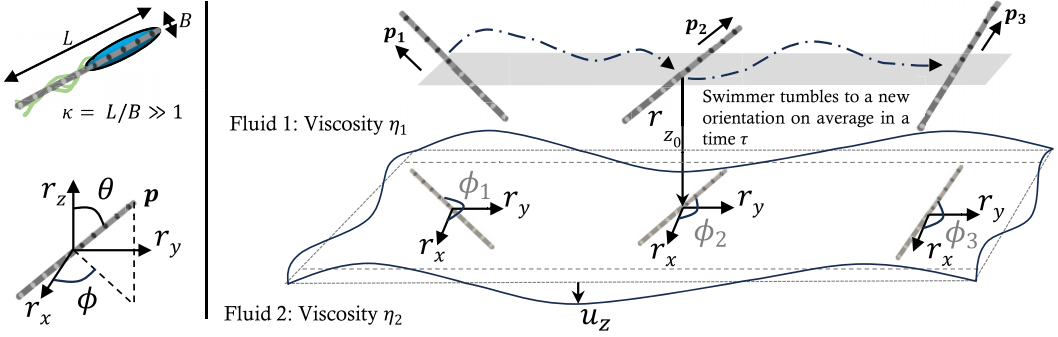


FIG. 1. A schematic of the system for tumbling swimmers: A swimmer disturbs the fluid in fluid region 1. A deformable interface separates regions 1 and 2 with viscosities  $\eta_1$  and  $\eta_2$ , respectively. The gray (dashed) plane represents the reference configuration of the undeformed interface and the black (solid) plane is the deformed configuration due to the disturbance flow field generated by the swimmer. On average, the swimmer spends a time  $\tau$  between two orientation tumbles, and after tumbling it intrinsically adopts a new orientation. Here,  $\mathbf{p}_i$  represents the swimmer orientations before the  $i$ th tumble and is decomposed in the coordinate system described in the bottom left corner. The lighter swimmers are the in-plane projections on the interface of the corresponding swimmer located above them in fluid 1. The top left figure shows how the slender swimmer model relates to an actual swimmer of length  $L$ .

for the velocity field  $\mathbf{v}_i$  and pressure field  $P_i$ , where  $i \in [1, 2]$ . Equation (1) is rendered nondimensional by scaling length by the swimmer length  $L$ , velocity by the characteristic disturbance velocity field of the swimmer  $V_s$ , and stress by  $\eta_1 V_s / L$ , where  $\eta_i$  is the viscosity; note that  $\lambda = \eta_2 / \eta_1$  is the viscosity ratio. The integral forcing on the right-hand side of Eq. (1a) represents the disturbance velocity field generated by the swimmer activity and is characterized by a dipole strength  $D < 0 (> 0)$  for pushers (pullers), the swimmer aspect ratio  $\kappa$ , and the swimmer orientation  $\mathbf{p}$ , where  $\mathbf{p}$  is expressible as  $\mathbf{p} \equiv p_x \mathbf{1}_x + p_y \mathbf{1}_y + p_z \mathbf{1}_z = \sin \theta \cos \phi \mathbf{1}_x + \sin \theta \sin \phi \mathbf{1}_y + \cos \theta \mathbf{1}_z$  in a Cartesian coordinate system (see Fig. 1).

The solution to Eq. (1) requires imposing boundary conditions both at the interface and on the swimmer surface. The boundary conditions on the deformable interface are the impenetrability ( $v_{1z}|_{r_{z_0}^+} = v_{2z}|_{r_{z_0}^-}$ ) and the no-slip velocity boundary conditions ( $\mathbf{v}_1 \cdot [\mathbf{I} - \mathbf{1}_z \mathbf{1}_z]|_{r_{z_0}^+} = \mathbf{v}_2 \cdot [\mathbf{I} - \mathbf{1}_z \mathbf{1}_z]|_{r_{z_0}^-}$ ); continuity of tangential stress ( $\sigma_{1-zx}(zy)|_{r_{z_0}^+} = \lambda \sigma_{2-zx}(zy)|_{r_{z_0}^-}$ ); the normal stress jump at the interface due to surface tension and elastic bending; and, finally, the kinematic boundary condition, noting that the interface is a material surface. Here, the stress  $\sigma_{i-z\alpha} = \partial v_{i-z} / \partial r_\alpha + \partial v_{i-\alpha} / \partial r_z$  for  $\alpha \in [x, y]$ . The kinematic and the normal stress boundary conditions, which involve the interface deformation  $u_z$ , are

$$\frac{\partial u_z}{\partial t} + \left( \frac{\eta_1 V_s L^2}{\kappa \beta} \right) \mathbf{v} \cdot \nabla_{r_\parallel} u_z = \left( \frac{\eta_1 V_s L^2}{\kappa \beta} \right) [v_z|_{u_z}] \quad \text{and} \quad (2a)$$

$$-(P_1|_{r_{z_0}^+} - P_2|_{r_{z_0}^-}) + 2 \left( \frac{\partial v_{1z}}{\partial r_z} \Big|_{r_{z_0}^+} - \lambda \frac{\partial v_{2z}}{\partial r_z} \Big|_{r_{z_0}^-} \right) = -\frac{\gamma}{\eta_1 V_s} \Delta_{r_\parallel} u_z + \frac{\kappa \beta}{\eta_1 V_s L^2} \Delta_{r_\parallel}^2 u_z, \quad (2b)$$

where  $\kappa \beta$  is the bending modulus,  $\gamma$  is the isotropic surface-tension of the deformable interface, and  $\Delta_{r_\parallel}$  denotes the Laplacian in the  $r_x - r_y$  plane. In Eq. (2a),  $t_c = \eta_1 L^3 / \kappa \beta$  is chosen as a timescale.

When a swimmer is at  $O(1)$  distances from the interface, we can simplify the nonlinear kinematic boundary condition using the asymptotics appropriate to a slender swimmer model. We note that, to leading order, the disturbance velocity field scales as  $O(\ln \kappa)^{-1}$ , due to the integral forcing in Eq. (1a), and is therefore asymptotically small for the swimmer ( $\kappa \gg 1$ ). Therefore, the boundary

TABLE I. The dimensional and nondimensional parameters of the system with their values and ranges specified.

Viscosity of fluid region $i$	$\eta_i$	
Bending modulus	$\kappa_\beta$	
Surface tension	$\gamma$	
Swimmer length	$L$	
Swimmer disturbance velocity	$V_s$	
Swimmer aspect ratio	$\kappa$	10
Swimmer dipole strength	$D$	-1
Ratio of surface tension to bending stress	$\Gamma = \gamma L^2 / \kappa_\beta$	1
Ratio of viscous stress to elastic stress	$\eta_1 V_s L^2 / \kappa_\beta$	1
Swimmer rotational diffusivity	$D_r$	6.67
Swimmer mean run duration	$\tau$	0.15–1
Viscosity ratio	$\lambda = \eta_2 / \eta_1$	0.1–10

conditions relating  $u_z$  and  $\mathbf{v}$  in Eqs. (2) allow us to similarly expand  $u_z$  as a series in powers of  $(\ln \kappa)^{-1}$ , from which we seek only the leading order term. This yields a linearized version of the kinematic boundary condition:

$$\frac{\partial u_z}{\partial t} \approx \left( \frac{\eta_1 V_s L^2}{\kappa_\beta} \right) v_z \Big|_{r_{z_0}}. \quad (3)$$

Now, the swimmer motion is coupled to the fluid velocity and interface deformation field via the force- and torque-free conditions on the swimmer, which yield its translation velocity  $\mathbf{V}^T$  and the rotation rate  $\dot{\mathbf{p}}$  respectively, and are

$$\mathbf{V}^T = \int_{-\frac{1}{2}}^{\frac{1}{2}} \mathbf{v}(s\mathbf{p}) ds \quad \text{and} \quad (4a)$$

$$\dot{\mathbf{p}} = 12 \int_{-\frac{1}{2}}^{\frac{1}{2}} (\mathbf{I} - \mathbf{p}\mathbf{p}) \cdot \mathbf{v}(s\mathbf{p}) s ds. \quad (4b)$$

The above set of linear equations and the boundary conditions are solved using two-dimensional Fourier transforms [21]. In Appendix A, we provide the expressions for the swimmer translation velocity, the rotation rate, and the boundary deformation equation. We express the relative importance of surface tension and bending stress through the parameter  $\Gamma \equiv \gamma L^2 / \kappa_\beta$  [see Eq. (A2)].

As stated at the beginning of the section, we superpose on this hydrodynamic framework the role of intrinsic stochastic reorientations by the swimmer via orientation tumbling and rotational Brownian motion (see Appendix B for details). For simplicity, we restrict these intrinsic reorientations to be in the plane of the undeformed interface, shown in Fig. 1 for tumbling; we rationalize this choice *a posteriori* in Sec. V. This implies that the swimmer exhibits a random change in the component of its orientation in the plane of the undeformed interface  $\phi$  (the reference plane), on average in a time interval  $\tau$  for tumbling and continuously by  $O(D_r)^{1/2}$  for active Brownian rotations. Here,  $\tau$  is the mean duration between tumbles, and  $D_r$  is the rotational diffusion coefficient. Therefore, in addition to the timescale of the relaxation of the interface deformation, there is an additional scale associated with the intrinsic swimmer reorientations, and the dynamics depends on a competition between these two effects. For simplicity, the undeformed flat interface is chosen as the initial condition.

The parameters discussed above are summarized in Table I. For a swimmer at unit length from the interface  $r_{z_0} = 1$ , we present results for the following set of parameters: the swimmer aspect ratio  $\kappa = 10$ , the ratio of viscous to bending stress  $\eta_1 V_s L^2 / \kappa_\beta = 1$ , and the ratio of surface tension to bending stress  $\Gamma = 1$ . Varying these parameters does not qualitatively affect the results, although we

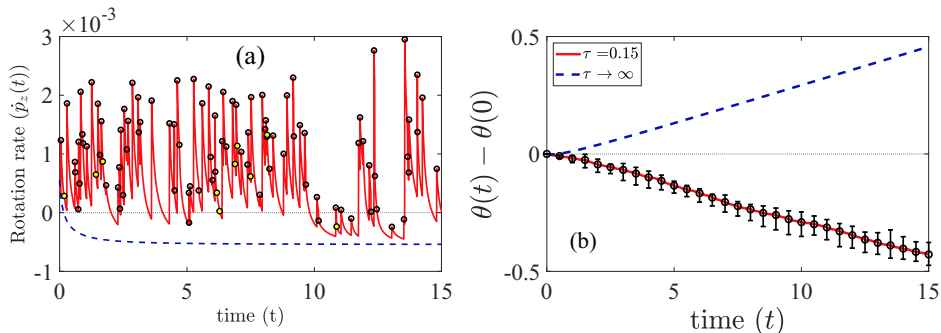


FIG. 2. (a) The vertical component of the rotation rate  $\dot{p}_z(t)$  plotted as a function of time for a tumbling ( $\tau = 0.15$ ) and straight ( $\tau \rightarrow \infty$ ) pusher initially oriented at  $\theta(0) = 70^\circ$ ,  $\phi(0) = 0^\circ$ . The black (open) circles denote tumbling events and the yellow (filled) circles denote those tumbles where  $\Delta\phi < \pm 20^\circ$  upon tumbling. (b) The relative orientation  $[\theta(t) - \theta(0)]$  plotted as a function of time averaged over five different runs; the error bars indicate the extremities associated with the individual runs. In all plots,  $r_{z_0} = 1$ ,  $\lambda = 0.1$ ,  $\kappa = 10$ ,  $\Gamma = 1$ , and  $\eta_1 V_s L^2 / \kappa_\beta = 1$ .

note that the validity of the asymptotics of the hydrodynamic flow field requires that  $\eta_1 V_s L^2 / \kappa_\beta < O(1)$  to apply the linearized kinematic boundary condition Eq. (3) [21].

### III. ROTATION AND TRANSLATION OF TUMBLING MICROSWIMMERS

If the swimmer orientation is neither parallel nor perpendicular to the plane of the undeformed interface, the hydrodynamic interactions outlined in Sec. II drive both swimmer translation and rotation relative to the interface [21]. Otherwise, due to symmetry, there is only translation. For a swimmer lacking intrinsic reorientation, or a straight swimmer (mean run duration  $\tau \rightarrow \infty$ ), the coupled hydrodynamics yield a rotation preference towards a parallel alignment in the long-time limit. However, when the swimmer is in the more viscous fluid (viscosity ratio  $\lambda < 1$ ), the short-time response is opposite to the long-time response, implying that the swimmer rotates in the opposite sense on the short interface relaxation time scales [21]. Therefore, to understand these processes we now focus on a system where  $\lambda = 0.1$ .

#### A. Effect of in-plane orientation tumbling on out-of-plane rotation of swimmers

In Fig. 2, we plot the time evolution of the rotation rate,  $\dot{p}_z$ , and the relative orientation,  $\theta(t) - \theta(0)$ , of a tumbling microswimmer that is initially at an orientation of  $\theta(0) = 70^\circ$ ,  $\phi(0) = 0^\circ$ . Figure 2(a) shows that the quasisteady  $\dot{p}_z$  for a straight swimmer is negative, resulting in  $\theta(t)$  increasing in time, as shown in Fig. 2(b). Note the signed relation between and the angular velocity  $\dot{\theta}$  and  $\dot{p}_z$  viz.,  $\dot{p}_z = d \cos \theta / dt = -\sin \theta \dot{\theta}$  [12,27]. However, for a tumbling swimmer,  $\dot{p}_z$  changes after every tumble event, such that it exhibits a new peak that we interpret as follows. After a tumble, there is a sudden change in the disturbance flow field that conforms to the randomly chosen new in-plane swimmer orientation  $\phi$  due to the instantaneous Stokes component of the hydrodynamics, thereby yielding the peaks. This is followed by a relaxation due to the interface deformation part of the hydrodynamics, which has responded to the new swimmer orientation.

In the random tumbling process, the swimmer chooses a new  $\phi$  randomly, such that  $\phi_{\text{post}} \in [0^\circ, 360^\circ]$ , where the subscript refers to post-tumble. When tumbling does not appreciably modify the rotational character by changing the disturbance field, the post-tumble orientation must be near the pretumble orientation. As a convenient choice, we consider small angular deviations to be those where  $\Delta\phi < \pm 20^\circ$  between two reorientations. In the realization shown in Fig. 2(a), less than 11% of tumbles involve  $\phi_{\text{post}} - \phi_{\text{pre}} < \pm 20^\circ$ , as expected for a random tumbling process. Therefore,

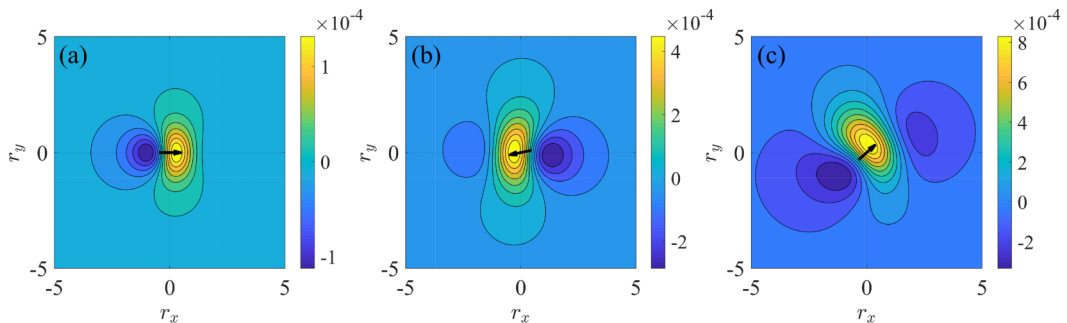


FIG. 3. Contour plots of the interface deformation (a) before the first tumble, (b) after two tumbles, and (c) after three tumbles, for swimmers initially oriented at  $\theta(0) = 70^\circ$ ,  $\phi(0) = 0^\circ$ . The black arrow represents the in-plane projection of the swimmer orientation. In all plots,  $r_{z0} = 1$ ,  $\lambda = 0.1$ ,  $\tau = 0.15$ ,  $\kappa = 10$ ,  $\Gamma = 1$ , and  $\eta_1 V_s L^2 / \kappa_\beta = 1$ .

owing to the flow fields developed by large swimmer angular deviations, new peaks in  $\dot{p}_z$  are dominantly positive. In fact, for  $\phi_{\text{post}} - \phi_{\text{pre}} > \pm 20^\circ$ , these new peaks in  $\dot{p}_z$  can even be higher than those in response to a flat interface. In turn, the total time trace of the rotation rate in any given time interval remains positive and  $\theta(t)$  decreases with time as shown in Fig. 2(b). Therefore, in contrast to a straight swimmer, the rotational response of a tumbling swimmer can promote rotation away from the deformable interface.

To understand the role of tumbling in modifying the disturbance flow field, in Fig. 3 we plot the contours of the interface deformation which, through the kinematic and normal stress boundary condition, connect the deformation to the disturbance field [19–21]. In the absence of tumbling, we are solving an initial value problem (IVP) in which the initial interface configuration is undeformed. As shown in Fig. 3(a), the disturbance field of the swimmer yields an interface deformation that has fore-aft asymmetry and left-right symmetry relative to the swimmer. The quasisteady negative  $\dot{p}_z$  of straight swimmers is a consequence of this configuration of the deformation. However, tumbling truncates the evolution of this IVP, following which the swimmer abruptly modifies its in-plane orientation. Subsequently, the interface must respond to the disturbance flow field of the new in-plane swimmer orientation, thereby initiating a new IVP. In this new IVP, the initial configuration of the interface (to which the swimmer is also responding simultaneously) is pre-stressed, unlike at time  $t = 0$ . This tumbling induced deformation field [see Figs. 3(b) and 3(c)] results in a modification of the flow field, which suppresses the approach to a quasisteady negative  $\dot{p}_z$ , as in the case of straight swimmers.

Therefore, despite the exponential decay in time of the rotation rate until the next tumble,  $\dot{p}_z$  of tumbling swimmers remains positive for longer times. The above argument suggests that an increase in the tumbling frequency would enable  $\dot{p}_z(t)$  to be positive for a longer time window by decreasing the time available for the disturbance flow field to relax. In Fig. 4(a), we plot the time evolution of the rotation rate  $\dot{p}_z$  for different values of  $\tau$ . For  $\tau = 0.15, 0.25$ , and  $1$ ,  $\dot{p}_z < 0$  for time intervals of 3.64, 5.39, and 12.55, respectively; the shortest times for the shortest timescales  $\tau$ . In turn, as shown in Fig. 4(b), the relative orientation of the swimmer decreases most rapidly for  $\tau = 0.15$ . Interestingly, Fig. 4(b) also highlights the fact that a tumbling swimmer can maintain a nearly stationary polar angle (see, for instance, the curve for  $\tau = 0.75$ ).

In Fig. 5(a), we plot the relative orientation of the swimmer for different initial swimmer orientations. For  $\tau = 0.15$ ,  $\theta(t)$  decreases for  $\theta(0) \gtrsim 55^\circ$  and increases for smaller initial orientations. Such a characteristic initial orientation dependent rotation of a tumbling swimmer is anticipated because relaxation of the hydrodynamic-interaction induced swimmer rotation rate depends on its orientation relative to the interface; becoming faster as  $\theta \rightarrow 0$  [21].

The orientation-dependent modification of the out-of-plane rotation for tumbling swimmers has a robust interpretation if we plot  $\dot{p}_z$  as a function of  $p_z$  for a straight-swimming microswimmer,

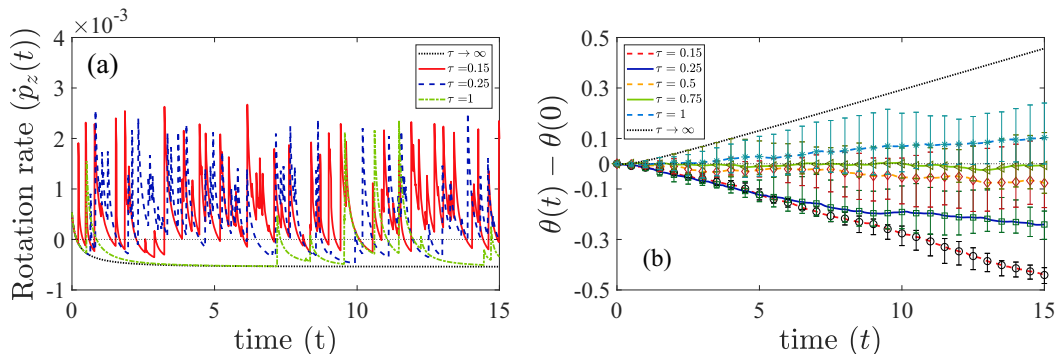


FIG. 4. (a) A single realization of the rotation rate  $\dot{p}_z$  plotted as a function of time for  $\theta(0) = 70^\circ$ ,  $\phi(0) = 0^\circ$  with mean run durations  $\tau = 0.15, 0.25, 1$ , and  $\tau \rightarrow \infty$ . (b) The relative rotation  $\theta(t) - \theta(0)$  of a pusher plotted as a function of time for the same swimmer initial orientation for  $\tau = 0.15, 0.25, 0.5, 0.75, 1$ , and  $\tau \rightarrow \infty$ , averaged over five runs; the error bars indicate the extremities associated with the individual runs. In all plots,  $r_{z0} = 1$ ,  $\lambda = 0.1$ ,  $\kappa = 10$ ,  $\Gamma = 1$ , and  $\eta_1 V_s L^2 / \kappa_\beta = 1$ .

as shown in Fig. 5(b). Any positive (negative) trajectory implies rotation away from (towards) the interface. At  $t = \tau = 0.15$ , the trajectory cuts across  $\dot{p}_z = 0$  and is positive for orientations greater than  $\theta \approx 60^\circ$ . For smaller initial orientations, a mean run duration of  $\tau = 0.15$  is too long for  $\dot{p}_z(t)$  to remain positive for at least half the duration of a given time interval. That is, the hydrodynamics evolves more rapidly than the tumbling induced cutoff of the evolution. For instance,  $\dot{p}_z(t) < 0$  for about 9.7, 7.48, and 6.55 time units, in an interval of 15 nondimensional time units for  $\theta(0) = 50^\circ, 55^\circ$ , and  $60^\circ$ , shown in Fig. 5(a), thereby yielding a net increase in the swimmer out-of-plane orientation with time for the former.

We note that while orientation tumbling needs to be more rapid for smaller swimmer orientations, nonetheless any finite  $\tau$  will suppress the tendency to align parallel relative to that of a straight swimmer.

### B. Effect of in-plane orientation tumbling on out-of-plane swimmer translation

The translation of a straight swimmer relative to a deformable interface due to hydrodynamic interactions is dependent on its relative orientation. Following an initial transient, for quasisteady

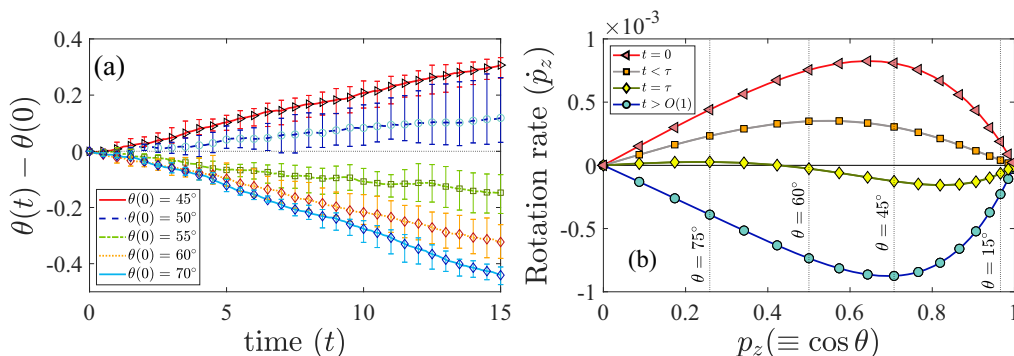


FIG. 5. (a) The relative rotation  $\theta(t) - \theta(0)$  of a pusher plotted as a function of time for different initial swimmer orientations at  $\tau = 0.15$  and  $\lambda = 0.1$ . The curves are averages of five different runs and the error bars indicate the extremities associated with the individual runs. (b) The orientation phase portrait of a straight swimmer for  $\lambda = 0.1$ . In all plots,  $r_{z0} = 1$ ,  $\kappa = 10$ ,  $\Gamma = 1$ , and  $\eta_1 V_s L^2 / \kappa_\beta = 1$ .

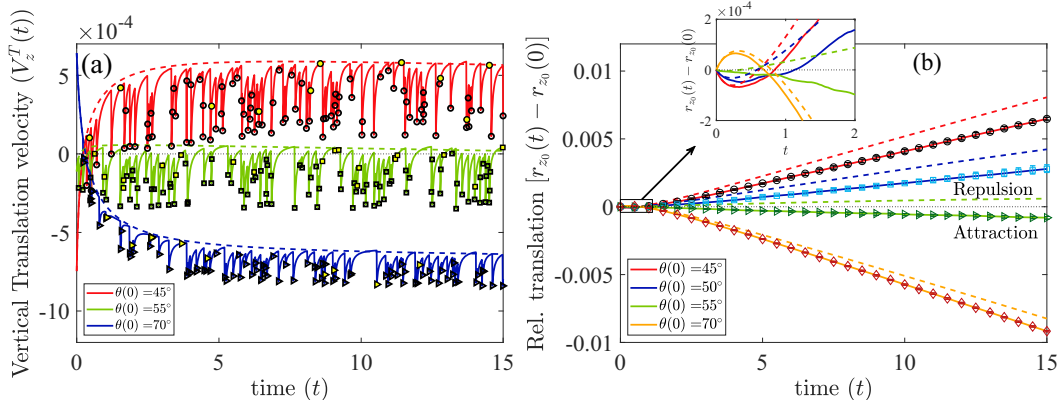


FIG. 6. (a) A single instance of the vertical translation velocity  $V_z^T$  of a pusher plotted as a function of time for initial swimmer orientations of  $\theta(0) = 45^\circ$ ,  $55^\circ$ , and  $70^\circ$  at  $\tau = 0.15$  and  $\lambda = 0.1$ . The black (open) markers denote tumbling events and the yellow (filled) markers denote those tumbles where  $\Delta\phi < \pm 20^\circ$  upon tumbling. (b) The relative vertical translation  $r_z(t) - r_z(0)$  for initial orientations  $\theta(0) = 45^\circ$ ,  $50^\circ$ ,  $55^\circ$ , and  $70^\circ$ . The solid curves are averages of five different runs and the error bars indicate the extremities associated with the individual runs. In both (a) and (b), the dashed curves correspond to straight swimmers ( $\tau \rightarrow \infty$ ). In all plots,  $r_{z0} = 1$ ,  $\kappa = 10$ ,  $\Gamma = 1$ , and  $\eta_1 V_s L^2 / \kappa \beta = 1$ .

translation the shift from attraction to repulsion occurs at an orientation of  $\theta_c \approx 55^\circ$ . Therefore, if  $\theta(t) < \theta_c$ , a pusher (puller) is repelled (attracted) from (towards) the interface, following an initial transient of opposite character.

In Fig. 6(a), we plot the vertical translation velocity of a tumbling swimmer for initial orientations of  $\theta(0) = 45^\circ$ ,  $55^\circ$ , and  $70^\circ$ , which straddle  $\theta_c$ . In contrast to rotation, where orientation tumbling indirectly suppresses swimmer translation towards the interface, by enabling rotation away from the interface, stronger swimmer translation towards the interface is facilitated. That is, the peaks in Fig. 6(a) corresponding to a tumbling event are inverted. Note that the exponential decay of the translation velocity between tumbles with  $\Delta\phi < \pm 20^\circ$  either continues to decay similarly to that of the pretumble orientation, or the post-tumble peaks appear close to the pretumble values. This was also the case for the rotation rate in Sec. III A. For swimmer orientations far from  $\theta_c$ , the long- and short-time translation character of a tumbling swimmer follows the straight-swimmer trajectory with a relative negative shift, as shown in Fig. 6(b) for  $\theta(0) = 45^\circ$ ,  $50^\circ$ , and  $70^\circ$ . Here,  $V_z^T$  of both tumbling- and straight-swimmers have the same sign convention, and the magnitude of both are comparable [see Fig. 6(a)].

However, as  $\theta \rightarrow \theta_c$ , the translation character is opposite for the two swimmers. For instance, for  $\theta(0) = 55^\circ$  in Fig. 6(b), a tumbling swimmer translates towards the interface, whereas the corresponding straight swimmer is repelled from the interface. Here, the magnitude of the negative  $V_z^T$  at short-times is larger than that at long times, where for  $t > O(1)$ ,  $V_z^T|_{\text{straight}} \rightarrow 0^+$ , and thus the short-time character dominates the migration response. As discussed in Sec. III A, for  $\tau = 0.15$ , tumbling is sufficiently rapid to hinder the relaxation of the hydrodynamic flow field for  $\theta(0) = 55^\circ$ . In turn, for  $\theta(0) = 55^\circ$  the swimmer translation follows a sequence of its short-time attraction [see inset of Fig. 6(b)].

### C. Effect of in-plane orientation tumbling on swimmer migration

Having studied the impact of the swimmer rotation and translation in isolation, we now consider how both influence the swimmer migration. In Fig. 7, we show the relative rotation and translation of a straight and tumbling swimmer that is initially oriented at  $\theta(0) = 56^\circ$ , with a mean run duration  $\tau = 0.15$  for the latter. We first interpret the response of a straight-swimming microswimmer (green

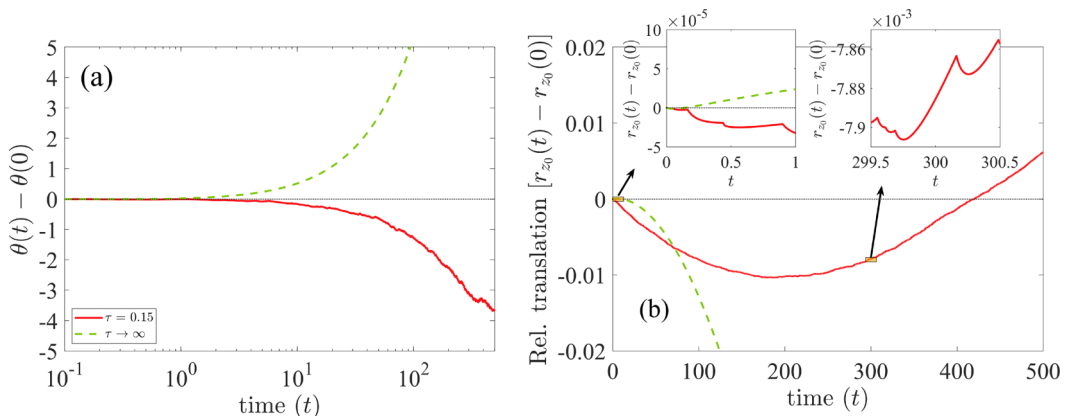


FIG. 7. (a) The relative rotation  $\theta(t) - \theta(0)$  of a pusher plotted as a function of time for  $\theta(0) = 56^\circ$ . (b) The corresponding relative vertical translation  $r_z(t) - r_z(0)$  plotted as a function of time. In both (a) and (b), the dashed curve corresponds to straight swimmers ( $\tau \rightarrow \infty$ ) and the solid curve is for a tumbling swimmer with  $\tau = 0.15$ . In all plots,  $r_{z_0} = 1$ ,  $\lambda = 0.1$ ,  $\kappa = 10$ ,  $\Gamma = 1$ , and  $\eta_1 V_s L^2 / \kappa_\beta = 1$ .

curve in Fig. 7). Owing to the short-time response for  $\theta = 56^\circ$ , a straight-swimming microswimmer is initially attracted towards the interface and is then repelled at intermediate times, corresponding to the quasisteady character for the same orientation. At this intermediate time, while  $\theta(t)$  is increasing, it is still in the vicinity of  $\theta(t) \approx 56^\circ$  [see left inset of Fig. 7(b)]. For longer times,  $\theta(t)$  increases to orientations whose long-time translation character is attraction, and thus the swimmer translates towards the interface. Therefore, the swimmer-interface coupled hydrodynamics produces a reentrant translation character of attraction-repulsion-attraction at short-intermediate-long times.

The migration character is quite different for a rapidly tumbling swimmer. For a mean duration between tumbles of  $\tau = 0.15$ , orientation tumbling continues to rotate the swimmer away from the interface, albeit much more slowly than the straight swimmer rotating towards the interface. For short times, the translation character for this orientation is attraction towards the interface as discussed in Sec. III B for  $\theta \approx \theta_c$  [see left inset of Fig. 7(b)], and continues until the swimmer orientation decreases by  $\Delta\theta \gtrsim 2^\circ$ . On further rotation of the swimmer away from the interface, the faster evolving orientation dependent hydrodynamics begins to dominate despite the cutoff that tumbling imposes [see right inset of Fig. 7(b)]. Therefore, a tumbling swimmer undergoes an interfacial attraction followed by repulsion.

#### IV. COMPARISON AND CONTRAST WITH ROTATIONAL BROWNIAN REORIENTATIONS

Thus far, we have analyzed how the orientation tumbles of swimmers influence the evolution of the hydrodynamic flow field, and thereby swimmer migration. Given the competing timescales in the problem, it is prudent to identify the regime in which the above analysis holds. In general, the swimmers are motile and the timescales associated with swimming a distance of order their own size is  $t_{\text{swim}} \equiv O(L/V_s) \sim O(1)s$ , for  $L \sim 6 - 8 \mu\text{m}$  and  $V_s \sim 10 \mu\text{m/s}$  [11, 28, 29]. We note that the timescale on which a swimmer in the vicinity of a *nondeforming* interface in a Newtonian fluid responds to rotation by the dipolar disturbance field it generates is the same, that is,  $t_{\text{Stokes}} \equiv O(L/V_s)$  [12]. Therefore, the Stokes hydrodynamic flow field developed when a swimmer is at a distance of  $O(L)$  from a flat interface can result in  $O(1)$  angular deviations in the time it takes to swim its own body length; although the constant prefactor ensures that the deviations are small. Additionally, for a deforming interface there is a deformation relaxation timescale in response to the disturbance field generated by the swimmer, which is  $t_{\text{interf}} \equiv O(\eta_1 L^3 / \kappa_\beta)$  [21]. For membranes,  $\kappa_\beta \sim 10 k_B T$ , where  $k_B$  is Boltzmann's constant and  $T$  is the temperature, implying  $t_{\text{interf}} \gtrsim O(1)s$

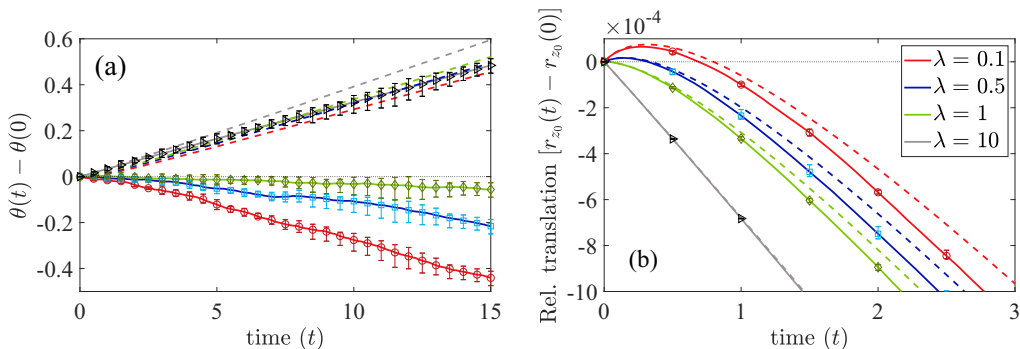


FIG. 8. (a) The relative rotation  $\theta(t) - \theta(0)$  of a pusher plotted as a function of time for  $\theta(0) = 70^\circ$  for viscosity ratio  $\lambda = 0.1, 0.5, 1, 10$ . (b) The corresponding relative vertical translational  $r_z(t) - r_z(0)$  plotted as a function of time. In both (a) and (b), the dashed curves correspond to straight swimmers ( $\tau \rightarrow \infty$ ) and the solid curves are averages of five different runs for  $\tau = 0.15$ ; the error bars indicate the extremities associated with the individual runs. In all plots,  $r_{z_0} = 1$ ,  $\lambda = 0.1$ ,  $\kappa = 10$ ,  $\Gamma = 1$ , and  $\eta_1 V_s L^2 / \kappa_\beta = 1$ .

[30,31]. Finally, the orientation tumbles occur on time scales of a mean duration  $t_{\text{intrin}} \equiv O(\tau)s$  [23]. Of these four time scales, the analysis presented in Sec. III neglects swimming, and we thereby neglect  $t_{\text{swim}}$  for simplicity. In this respect, the model swimmer considered here is similar to the stresslet-mode squirmer [19,32] and is also referred to as a shaker in literature [33]. Furthermore, we have considered the regime where  $t_{\text{Stokes}} \approx t_{\text{interf}}$ , implying  $\eta_1 V_s L^2 / \kappa_\beta \sim O(1)$  as mentioned in Sec. II, and is of relevance to many biological systems involving motion near deformable boundaries [10,31,34]. Our focus here is on how swimmer stochasticity, acting on timescales characterized by  $t_{\text{intrins}}$ , influences the hydrodynamics, for which we treat swimmers that can rapidly reorient themselves.

We note that while the results discussed in Sec. III are for viscosity ratios  $\lambda < 1$ , the suppression of alignment parallel to the interface is itself not restricted to  $\lambda < 1$ , as shown in Fig. 8(a). For  $\lambda = 1$ , a swimmer oriented at  $\theta(0) = 70^\circ$  rotates weakly away for rapid tumbling with  $\tau = 0.15$ , although for  $\lambda = 10$ , the rotation is still towards the interface, albeit with a reduction in the magnitude of the rotation rate. However, as  $\lambda \rightarrow \infty$ , the deformation  $u_z \rightarrow 0$  and the interface approaches a planar

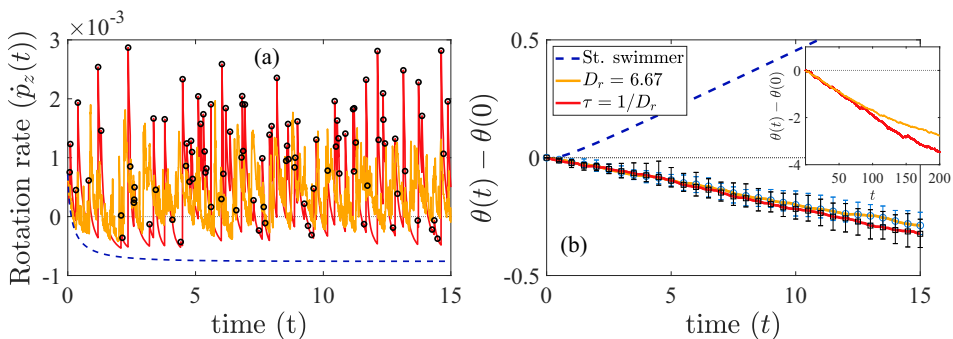


FIG. 9. (a) The vertical component of the rotation rate  $\dot{p}_z(t)$  plotted as a function of time for a tumbling ( $\tau = 0.15$ ), rotationally diffusing ( $D_r = 6.67$ ) and straight ( $\tau \rightarrow \infty$  or  $D_r \rightarrow 0$ ) pusher initially oriented at  $\theta(0) = 60^\circ$ ,  $\phi(0) = 0^\circ$ ; the black (open) circles mark tumbling events. (b) The relative orientation  $\theta(t) - \theta(0)$  for the same initial orientation averaged over five different runs plotted as a function of time; the error bars indicate the extremities associated with the individual runs. The inset of (b) shows the orientation change of a single realization over long times. In all plots,  $r_{z_0} = 1$ ,  $\lambda = 0.1$ ,  $\kappa = 10$ ,  $\Gamma = 1$ , and  $\eta_1 V_s L^2 / \kappa_\beta = 1$ .

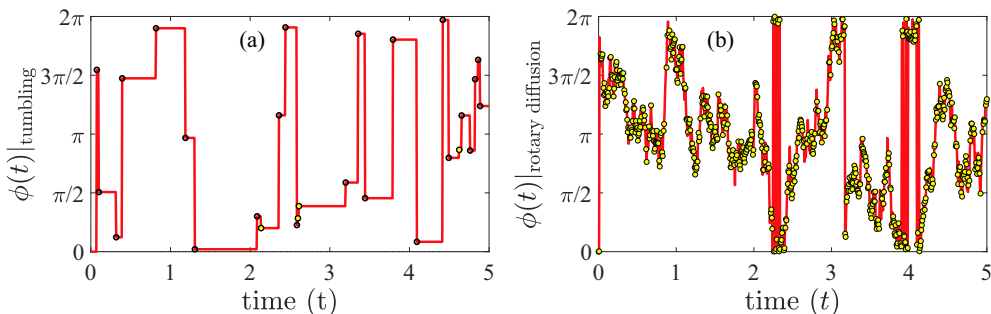


FIG. 10. The in-plane component of the swimmer orientation  $\phi(t)$  plotted as a function of time for a (a) tumbling and (b) rotationally diffusing pusher initially oriented at  $\theta(0) = 60^\circ$ ,  $\phi(0) = 0^\circ$ . The black (open) circles in (a) denote 27 tumbling events and the yellow (filled) circles denote those four tumbles where change in  $\phi < 20^\circ$  upon tumbling. The yellow circles in (b) show the 616/800 rotational diffusion events in which  $\Delta\phi \leq 20^\circ$ . In all plots,  $r_{z_0} = 1$ ,  $\lambda = 0.1$ ,  $\kappa = 10$ ,  $\Gamma = 1$ , and  $\eta_1 V_s L^2 / \kappa_\beta = 1$ .

configuration [see Eq. (A2)]. Therefore, while the translation of a pusher towards the interface due to tumbling continues to be enhanced independent of  $\lambda$ , as shown in Fig. 8(b), the gap between the two diminishes as  $\lambda \rightarrow \infty$ .

Importantly, another mechanism for self-propelled particles to exhibit intrinsic orientational stochasticity is by executing active Brownian rotations [24]. Unlike tumbling, which involves large abrupt changes in orientation interspersed with average durations of  $O(\tau)$  where only hydrodynamic effects apply, rotational Brownian motion results in orientation fluctuations at every time step in conjunction with hydrodynamics. The angular deviations in this case scales as  $O(D_r)^{1/2}$ , where  $D_r$  is the rotational diffusion coefficient (see Appendix B). In the following, we briefly compare the influence of the two reorientation mechanisms on the hydrodynamically induced reorientation.

For comparison, we consider the orientational response of the two swimmer types for  $D_r = 1/\tau = 6.67$  in Fig. 9. The rotation rate  $\dot{p}_z$  in Fig. 9(a) evolves slightly differently for the two mechanisms. Note that the peaks in  $\dot{p}_z$  for rotational diffusion are not as high as they are for tumbling. This is expected given the nonlocal nature of reorientations through tumbling as compared to rotational diffusion. In other words, in a random tumbling process, the post-tumble in-plane swimmer orientation can be  $\phi_{\text{post}} \in [0, 360^\circ]$ , whereas in rotational diffusion, the reorientations in the forward direction are more favorable. This aspect is made clear in Fig. 10, where we plot the time evolution of the in-plane component  $\phi$  of the swimmer orientation for a tumbling and a rotationally diffusing swimmer. In Fig. 10(a), only a small fraction of the tumbles yield a  $\Delta\phi < \pm 20^\circ$ . In contrast, Fig. 10(b) shows that rotational diffusion principally exhibits  $\Delta\phi < \pm 20^\circ$ . Thus, following the rationale described in Sec. III A, the out-of-plane angular deviation away from the interface is larger for tumbling in Fig. 9(b) (see inset). Nevertheless, both reorientation mechanisms enhance rotation away from the interface.

## V. CONCLUSION

We have examined how intrinsic stochastic reorientations executed by an orientable microswimmer play an important role in its hydrodynamically induced migration near a deformable interface. We have shown that orientation tumbles or active rotational diffusion compete with interfacial deformation, thereby enabling a pusher to migrate away from the interface by modifying its rotational response. While we have formulated the hydrodynamics in three dimensions, we restricted the intrinsic swimmer reorientation to be in the plane of the undeformed interface. This assumes that a swimmer at distances of order its own size from a boundary is more likely to reorient itself in the plane of the boundary, which was also found in recent experiments [35,36]. This suggests

that microswimmers executing orientation tumbles can exhibit slightly stronger hydrodynamic reorientations relative to deformable interfaces than those executing active rotational diffusion. Such planar tumbles, interspersed with out-of-plane tumbles, can influence the overall swimmer migration relative to the interface and may also be important in studies involving optimal swimmer navigation strategies [37].

We have only scraped the surface of the multiscale parameter regime for the interaction between microswimmers and deformable boundaries. Clearly, our results may have bearing on microswimmers in a variety of confinements, such as those involving motion of mammalian sperm through compliant ducts [34,38]. Indeed, hydrodynamic interactions and orientational stochasticity can have consequences on the boundary accumulation or depletion of microswimmers at long times [12,13], and influence other effects impacting their rectification on shorter timescales [39,40], as well as their residence time near boundaries. Moreover, as noted above, experiments have shown that the residence time of motile bacteria near planar boundaries is correlated with their tumbling frequency [35,36]. Finally, we note that the nonlinear effects emerging from large boundary deformations and swimmer flexibility neglected here may become relevant as the swimmer approaches the boundary [41,42].

### ACKNOWLEDGMENTS

S.N. would like to thank N. Marath for useful discussions. The authors gratefully acknowledge support from the Swedish Research Council under Grant No. 638-2013-9243. Nordita is partially supported by Nordforsk.

### APPENDIX A: EXPRESSIONS FOR THE SWIMMER TRANSLATION VELOCITY AND ROTATION RATE

The expression for the vertical translation velocity  $V_z^T$  and rotation rate  $\dot{\mathbf{p}}$  of a slender microswimmer with orientation  $\mathbf{p}$  due to hydrodynamic interaction with a deformable interface are obtained by solving the equations and boundary conditions outlined in Sec. II. The translation velocity is expressible as

$$\begin{aligned}
 V_z^T = & -\left(\frac{\kappa_\beta}{\eta_1 V_s L^2}\right) \frac{1}{(1+\lambda)} \int d\mathbf{k} (4\pi^2 k^2 + \Gamma) \exp(2\pi k r_{z_0}) \hat{u}_z \left(\frac{1}{ip_l - p_z}\right) \\
 & \times \left[ \pi k p_z \cosh[\pi k(ip_l - p_z)] + \sinh[\pi k(ip_l - p_z)] \left(1 - 2\pi k r_{z_0} - \frac{p_z}{ip_l - p_z}\right) \right] \\
 & - \left(\frac{1-\lambda}{1+\lambda}\right) \frac{D}{\ln \kappa} \int d\mathbf{k} \frac{\exp(4\pi k r_{z_0})}{8\pi^2 k^2} \int_{-\frac{1}{2}}^{\frac{1}{2}} ds \exp(2\pi i k p_l s) \exp(-2\pi k s p_z) \\
 & \times \left\{ \pi k p_z \sinh[\pi k(ip_l + p_z)] (1 + 4\pi k(s p_z - r_{z_0})) + (1 - \cosh[\pi k(ip_l + p_z)]) \right. \\
 & \left. \times \left(1 + 2\pi k s p_z - 4\pi k r_{z_0} - 8\pi^2 k^2 r_{z_0} (s p_z - r_{z_0}) - \left(\frac{ip_l - p_z}{ip_l + p_z}\right) (1 + 4\pi k(s p_z - r_{z_0}))\right) \right\}, \\
 & \text{and} \tag{A1}
 \end{aligned}$$

where the interface deformation field is characterized by simultaneously solving

$$\begin{aligned}
 \frac{\partial \hat{u}_z}{\partial t} + \frac{\pi k}{1+\lambda} (\Gamma + 4\pi^2 k^2) \hat{u}_z = & -\left(\frac{\eta_1 L^2 V_s}{\kappa_\beta}\right) \frac{D}{(1+\lambda) \ln \kappa} \frac{\exp(2\pi k r_{z_0})}{4\pi^2 k^2} \left[ \pi k p_z \sinh[\pi k(ip_l + p_z)] \right. \\
 & \left. + \left(1 - 2\pi k r_{z_0} - \left(\frac{ip_l - p_z}{ip_l + p_z}\right)\right) (1 - \cosh[\pi k(ip_l + p_z)]) \right]. \tag{A2}
 \end{aligned}$$

Here,  $\hat{u}_z$  and  $\hat{v}$  are the Fourier-transformed interface deformation and disturbance flow fields,  $\Gamma = \gamma L^2 / \kappa_\beta$  represents the ratio of the surface tension  $\gamma$  to the bending stress,  $s \in [-1/2, 1/2]$  is the coordinate along the axial direction of the swimmer, and  $p_l$  and  $p_t$  are the components of the orientation longitudinal and transverse to wave vector  $\mathbf{k}$ , respectively.

The components of the swimmer rotation rate  $\dot{\mathbf{p}}$  are

$$\dot{p}_x = 12 \int d\mathbf{k} \int_{-\frac{1}{2}}^{\frac{1}{2}} ds s \exp(2\pi i k s p_l) [\hat{v}_{1x}(1 - p_x^2) - (\hat{v}_{1y} p_y p_x + \hat{v}_{1z} p_z p_x)], \quad (\text{A3})$$

$$\dot{p}_y = 12 \int d\mathbf{k} \int_{-\frac{1}{2}}^{\frac{1}{2}} ds s \exp(2\pi i k s p_l) [\hat{v}_{1y}(1 - p_y^2) - (\hat{v}_{1x} p_x p_y + \hat{v}_{1z} p_z p_y)], \quad \text{and} \quad (\text{A4})$$

$$\dot{p}_z = 12 \int d\mathbf{k} \int_{-\frac{1}{2}}^{\frac{1}{2}} ds s \exp(2\pi i k s p_l) [\hat{v}_{1z}(1 - p_z^2) - (\hat{v}_{1x} p_x p_z + \hat{v}_{1y} p_y p_z)], \quad (\text{A5})$$

where the  $x$  and  $y$  components of  $\hat{\mathbf{v}}_1$  can be expressed in terms of  $\hat{v}_{1l}$  and  $\hat{v}_{1t}$  as  $\hat{v}_{1x} = \hat{v}_{1l} k_x / k + \hat{v}_{1t} k_y / k$  and  $\hat{v}_{1y} = \hat{v}_{1t} k_y / k - \hat{v}_{1l} k_x / k$ . The normal and transverse velocity field components  $\hat{v}_{1z}$  and  $\hat{v}_{1t}$ , respectively, are

$$\begin{aligned} \hat{v}_{1z}|_{\text{hyd-int}} &= -\left(\frac{\kappa_\beta}{\eta_1 V_s L^2}\right) \frac{\pi k}{(1 + \lambda)} (4\pi^2 k^2 + \Gamma) [1 + 2\pi k(r_z - r_{z_0})] \exp(-2\pi k(r_z - r_{z_0})) \hat{u}_z \\ &\quad - \frac{D}{8\pi^2 k^2 \ln \kappa} \left(\frac{1 - \lambda}{1 + \lambda}\right) \exp(4\pi k r_{z_0}) \exp(-2\pi k r_z) \\ &\quad \times \left[ (1 - \cosh[\pi k(ip_l + p_z)]) \left(1 + 2\pi k r_z - 4\pi k r_{z_0} - 8\pi^2 k^2 r_{z_0} (r_z - r_{z_0})\right) \right. \\ &\quad \left. - \left(\frac{ip_l - p_z}{ip_l + p_z}\right) (1 + 4\pi k(r_z - r_{z_0}))\right) + \pi k p_z \sinh[\pi k(ip_l + p_z)] \\ &\quad \left. \times (1 + 4\pi k(r_z - r_{z_0}))\right]; \quad r_z \geq r_{z_0} \\ \hat{v}_{1t}|_{\text{hyd-int}} &= -\frac{1}{2\pi^2 k^2 \ln \kappa} \frac{D}{p_l^2 + p_z^2} \frac{p_t (ip_l - p_z)}{(1 + \lambda)} \exp(4\pi k r_{z_0}) \exp(-2\pi k r_z) \\ &\quad \times \sinh^2\left(\frac{\pi}{2} k(ip_l + p_z)\right), \end{aligned} \quad (\text{A6})$$

and  $\hat{v}_{1l} = (i/2\pi k) \partial \hat{v}_{1z} / \partial r_z$ .

## APPENDIX B: IMPLEMENTATION AND VALIDATION OF ORIENTATION TUMBLING AND ROTATIONAL DIFFUSION

We implement orientation tumbling in the plane of the undeformed interface, obeying Poisson's interval distribution [43]. At each time step, a uniform random number is generated in the interval  $[0, 1]$ . If this number is less than  $dt/\tau$ , then tumbling is a success. For successful tumbles, the in-plane orientation  $\phi$  is reset to a new random value between  $[0, 2\pi]$ .

Active Brownian rotations are implemented as a Wiener process in orientation space as follows. At each time step  $\Delta t$ , a random number  $\chi$  is generated from a normal distribution with zero mean and unit variance. The angular change is  $\Delta\phi = \sqrt{2D_r \Delta t} \chi$  [39,44] for a prescribed swimmer rotational diffusivity coefficient  $D_r$ .

In Fig. 11, we validate this approach by plotting the averaged in-plane orientation autocorrelation functions  $\langle \mathbf{p}_\parallel(t) \cdot \mathbf{p}_\parallel(0) \rangle$  and  $\langle [\mathbf{p}_\parallel(t) \cdot \mathbf{p}_\parallel(0)]^2 \rangle$ , where  $\mathbf{p}_\parallel(t) = \cos \phi(t) \mathbf{1}_x + \sin \phi(t) \mathbf{1}_y$ . Their

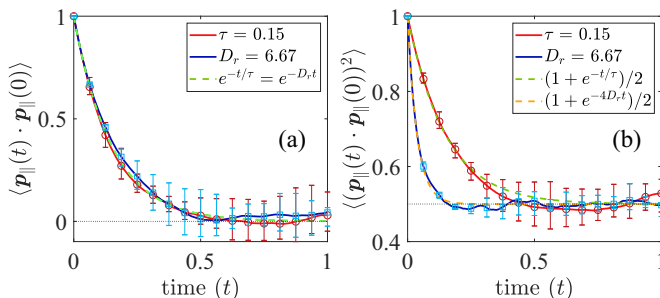


FIG. 11. The in-plane orientation autocorrelation functions (a)  $\langle \mathbf{p}_{\parallel}(t) \cdot \mathbf{p}_{\parallel}(0) \rangle$  and (b)  $\langle [\mathbf{p}_{\parallel}(t) \cdot \mathbf{p}_{\parallel}(0)]^2 \rangle$  plotted for both a tumbling ( $\tau = 0.15$ ) and a rotationally diffusing ( $D_r = 6.67$ ) swimmer averaged over five different runs; the error bars indicate the extremities associated with the individual runs. In both plots,  $\theta(0) = 70^\circ$ ,  $r_{z_0} = 1$ ,  $\lambda = 0.1$ ,  $\kappa = 10$ ,  $\Gamma = 1$ , and  $\eta_1 V_s L^2 / \kappa_\beta = 1$ .

analytical expressions for 2D reorientations are  $\langle \mathbf{p}_{\parallel}(t) \cdot \mathbf{p}_{\parallel}(0) \rangle = \exp(-t/t_{r1})$  and  $\langle [\mathbf{p}_{\parallel}(t) \cdot \mathbf{p}_{\parallel}(0)]^2 \rangle = [1 + \exp(-t/t_{r2})]/2$ , where  $t_{r1} = \tau$ ,  $1/D_r$  and  $t_{r2} = \tau$ ,  $1/(4D_r)$  for orientation tumbling and active Brownian rotations, respectively [45,46].

- 
- [1] A. Siryaporn, M. K. Kim, Y. Shen, H. A. Stone, and Z. Gitai, Colonization, competition, and dispersal of pathogens in fluid flow networks, *Curr. Biol.* **25**, 1201 (2015).
  - [2] S. Lee, J. W. M. Bush, A. E. Hosoi, and E. Lauga, Crawling beneath the free surface: Water snail locomotion, *Phys. Fluids* **20**, 082106 (2008).
  - [3] I. Sekirov, S. L. Russell, L. C. M. Antunes, and B. B. Finlay, Gut microbiota in health and disease, *Physiol. Rev.* **90**, 859 (2010).
  - [4] J. D. Wheeler, E. Secchi, R. Rusconi, and R. Stocker, Not just going with the flow: The effects of fluid flow on bacteria and plankton, *Annu. Rev. Cell Dev. Biol.* **35**, 213 (2019).
  - [5] T. Dalton, S. E. Dowd, R. D. Wolcott, Y. Sun, C. Watters, J. A. Griswold, and K. P. Rumbaugh, An in vivo polymicrobial biofilm wound infection model to study interspecies interactions, *PLoS ONE* **6**, e27317 (2011).
  - [6] G. D. Bixler and B. Bhushan, Biofouling: lessons from nature, *Phil. Trans. Royal Soc. A: Math., Phys. and Engg. Sci.* **370**, 2381 (2012).
  - [7] S. Martel, M. Mohammadi, O. Felfoul, Z. Lu, and P. Pouponneau, Flagellated magnetotactic bacteria as controlled MRI-trackable propulsion and steering systems for medical nanorobots operating in the human microvasculature, *Int. J. Robotics Res.* **28**, 571 (2009).
  - [8] D. D. Thomas, M. Navab, D. A. Haake, A. M. Fogelman, J. N. Miller, and M. A. Lovett, *Treponema pallidum* invades intercellular junctions of endothelial cell monolayers., *Proc. Natl. Acad. Sci. USA* **85**, 3608 (1988).
  - [9] A. J. A. McBride, D. A. Athanazio, M. G. Reis, and A. I. Ko, Leptospirosis, *Curr. Opin. Infect. Dis.* **18**, 376 (2005).
  - [10] T. J. Moriarty, M. U. Norman, P. Colarusso, T. Bankhead, P. Kubes, and G. Chaconas, Real-time high resolution 3D imaging of the lyme disease spirochete adhering to and escaping from the vasculature of a living host, *PLoS Path.* **4**, e1000090 (2008).
  - [11] E. Lauga, Bacterial hydrodynamics, *Annu. Rev. Fluid Mech.* **48**, 105 (2016).
  - [12] A. P. Berke, L. Turner, H. C. Berg, and E. Lauga, Hydrodynamic attraction of swimming microorganisms by surfaces, *Phys. Rev. Lett.* **101**, 038102 (2008).

- [13] L. Ning, X. Lou, Q. Ma, Y. Yang, N. Luo, K. Chen, F. Meng, X. Zhou, M. Yang, and Y. Peng, Hydrodynamics-induced long-range attraction between plates in bacterial suspensions, *Phys. Rev. Lett.* **131**, 158301 (2023).
- [14] P. S. Stewart, Mini-review: Convection around biofilms, *Biofouling* **28**, 187 (2012).
- [15] J. C. Conrad and R. Poling-Skutvik, Confined flow: Consequences and implications for bacteria and biofilms, *Annu. Rev. Chem. Biomol. Eng.* **9**, 175 (2018).
- [16] C. Montecucco and R. Rappuoli, Living dangerously: How *Helicobacter pylori* survives in the human stomach, *Nat. Rev. Mol. Cell Biol.* **2**, 457 (2001).
- [17] R. Ledesma-Aguilar and J. M. Yeomans, Enhanced motility of a microswimmer in rigid and elastic confinement, *Phys. Rev. Lett.* **111**, 138101 (2013).
- [18] M. A. Dias and T. R. Powers, Swimming near deformable membranes at low Reynolds number, *Phys. Fluids* **25**, 101901 (2013).
- [19] V. A. Shaik and A. M. Ardekani, Motion of a model swimmer near a weakly deforming interface, *J. Fluid Mech.* **824**, 42 (2017).
- [20] A. Daddi-Moussa-Ider, C. Kurzthaler, C. Hoell, A. Zöttl, M. Mirzakanloo, M.-R. Alam, A. M. Menzel, H. Löwen, and S. Gekle, Frequency-dependent higher-order stokes singularities near a planar elastic boundary: Implications for the hydrodynamics of an active microswimmer near an elastic interface, *Phys. Rev. E* **100**, 032610 (2019).
- [21] S. Nambiar and J. S. Wettlaufer, Hydrodynamics of slender swimmers near deformable interfaces, *Phys. Rev. Fluids* **7**, 054001 (2022).
- [22] M. Rey, G. Volpe, and G. Volpe, Light, matter, action: Shining light on active matter, *ACS Photonics* **10**, 1188 (2023).
- [23] H. Berg, *E. coli in Motion*, Biological and Medical Physics, Biomedical Engineering (Springer, New York, 2008).
- [24] C. Bechinger, R. Di Leonardo, H. Löwen, C. Reichhardt, G. Volpe, and G. Volpe, Active particles in complex and crowded environments, *Rev. Mod. Phys.* **88**, 045006 (2016).
- [25] T. V. Kasyap, D. L. Koch, and M. Wu, Hydrodynamic tracer diffusion in suspensions of swimming bacteria, *Phys. Fluids* **26**, 081901 (2014).
- [26] S. Nambiar, P. Garg, and G. Subramanian, Enhanced velocity fluctuations in interacting swimmer suspensions, *J. Fluid Mech.* **907**, A26 (2021).
- [27] D. Lopez and E. Lauga, Dynamics of swimming bacteria at complex interfaces, *Phys. Fluids* **26**, 071902 (2014).
- [28] N. C. Darnton, L. Turner, S. Rojevsky, and H. C. Berg, On torque and tumbling in swimming *Escherichia coli*, *J. Bacterio.* **189**, 1756 (2007).
- [29] R. E. Goldstein, Green algae as model organisms for biological fluid dynamics, *Annu. Rev. Fluid Mech.* **47**, 343 (2015).
- [30] U. Seifert, Configurations of fluid membranes and vesicles, *Adv. Phys.* **46**, 13 (1997).
- [31] J. B. Freund, Numerical simulation of flowing blood cells, *Annu. Rev. Fluid Mech.* **46**, 67 (2014).
- [32] J. R. Blake, A spherical envelope approach to ciliary propulsion, *J. Fluid Mech.* **46**, 199 (1971).
- [33] J. Stenhammar, C. Nardini, R. W. Nash, D. Marenduzzo, and A. Morozov, Role of correlations in the collective behavior of microswimmer suspensions, *Phys. Rev. Lett.* **119**, 028005 (2017).
- [34] E. Gaffney, H. Gadêlha, D. Smith, J. Blake, and J. Kirkman-Brown, Mammalian sperm motility: Observation and theory, *Annu. Rev. Fluid Mech.* **43**, 501 (2011).
- [35] M. Molaei, M. Barry, R. Stocker, and J. Sheng, Failed escape: Solid surfaces prevent tumbling of *Escherichia coli*, *Phys. Rev. Lett.* **113**, 068103 (2014).
- [36] G. Junot, T. Darnige, A. Lindner, V. A. Martinez, J. Arlt, A. Dawson, W. C. K. Poon, H. Auradou, and E. Clément, Run-to-tumble variability controls the surface residence times of *E. coli* bacteria, *Phys. Rev. Lett.* **128**, 248101 (2022).
- [37] A. Daddi-Moussa-Ider, H. Löwen, and B. Liebchen, Hydrodynamics can determine the optimal route for microswimmer navigation, *Commun. Phys.* **4**, 15 (2021).
- [38] F. L. J. and M. Amy, Sperm motility in the presence of boundaries, *Bull. Math. Biol.* **57**, 679 (1995).

- [39] G. Li and J. X. Tang, Accumulation of microswimmers near a surface mediated by collision and rotational Brownian motion, [Phys. Rev. Lett.](#) **103**, 078101 (2009).
- [40] K. Drescher, J. Dunkel, L. H. Cisneros, S. Ganguly, and R. E. Goldstein, Fluid dynamics and noise in bacterial cell–cell and cell–surface scattering, [Proc. Natl. Acad. Sci. USA](#) **108**, 10940 (2011).
- [41] S. Dalal, A. Farutin, and C. Misbah, Amoeboid swimming in a compliant channel, [Soft Matter](#) **16**, 1599 (2020).
- [42] S. Weady, D. B. Stein, A. Zidovska, and M. J. Shelley, Conformations, correlations, and instabilities of a flexible fiber in an active fluid, [Phys. Rev. Fluids](#) **9**, 013102 (2024).
- [43] H. C. Berg, *Random Walks in Biology* (Princeton University Press, Princeton, NJ, 2018).
- [44] A. Callegari and G. Volpe, Numerical simulations of active Brownian particles, in *Flowing Matter*, edited by F. Toschi and M. Sega (Springer International Publishing, Cham, 2019), pp. 211–238.
- [45] M. Doi and S. F. Edwards, *The Theory of Polymer Dynamics*, International Series of Monographs on Physics (Oxford University Press, Oxford, 1988), Vol. 73.
- [46] M. Sandoval, N. K. Marath, G. Subramanian, and E. Lauga, Stochastic dynamics of active swimmers in linear flows, [J. Fluid Mech.](#) **742**, 50 (2014).